Effect of Coating Defect Geometry and Orientation in AC Corrosion of Buried Pipelines – Laboratory Experiments

Andreas Junker-Holst (M.Sc., MetriCorr, Denmark)
Lars Vendelbo Nielsen (Ph.D., MetriCorr, Denmark)

Abstract
Coupons for investigation of AC corrosion on cathodically protected pipelines acts as artificial coating defects of a well-defined area of 1 cm^2, typically circular, according to the EN 15280:2013 Standard. This is convenient for current density calculations, but real life coating defects can be expected to have multiple sizes and geometries, which is known to affect critical parameters such as the spread resistance, AC and DC current density and ultimately the AC corrosion rate. The effect of size, geometry, length/width-ratio, coating thickness and defect orientation is investigated at different protection levels in the present study, using electrical resistance measurements (ER) and electrochemical impedance spectroscopy (EIS).
The findings suggests that smaller, scratch-like defects with a very thin adjacent coating yields the smallest spread and charge transfer resistance, and will therefore be more vulnerable to AC corrosion.
The coating defect orientation also has a large influence on the AC corrosion rate, with upwards pointing defects corroding the most, and downwards pointing defects corroding the least under identical AC and DC voltage control, suggesting that the spread resistance is affected by formed species at the surface, having another density than water, or having a directional diffusion dependency.

Introduction
Coupons for investigation of AC corrosion on cathodically protected pipelines are buried in the soil next to pipelines, and electrically connected to these. In this way, they act as artificial coating defects of a well-defined area and well-known defect geometry. Such coupons can be analysed to investigate the corrosion conditions on the pipe either after an experimental period, or in situ, using ER-technology. It is customary that such artificial coating defects have an area of 1cm^2, but real life coating defects can of course have multiple sizes and geometries, as well as orientation with respect to the pipe. This study investigates

- The effect of varying defect size on the spread resistance and on the AC and DC current density, which are identified as critical parameters when investigating AC corrosion [1] [2] [3].
- The effect of coating thickness known to cause a varied current density distribution across the defect surface, as well as the development of a pitting environment in defects having a large depth/width ratio [3] [4].
- The effect of varying the coating defect gradually from a circular defect to a scratch geometry having a width/length ratio of 1:100, while keeping the area constant, which influences the spread resistance [1].
- The effect of the defect orientation with respect to the pipe. Cathode reactions cause formation of hydrogen gas and hydroxyl-ions which are lighter and heavier than water respectively. Dependent on the orientation of the defect surface, these can be concentrated or transported away from the surface causing different chemical environments and thus corrosion conditions.

Figure 1 shows an overview over the variation of coating defects investigated in this study.

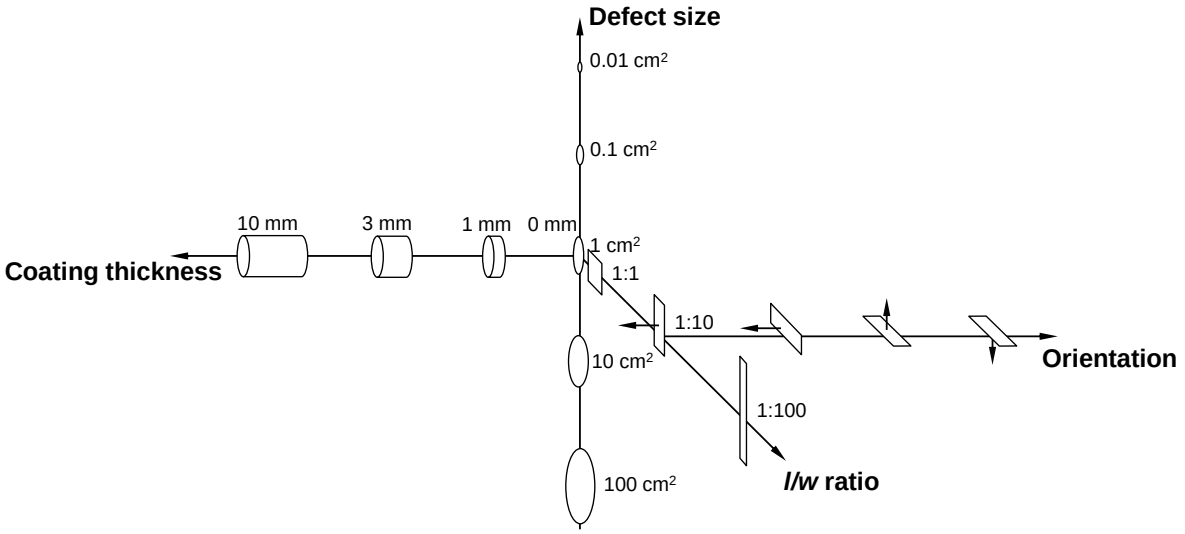

Figure 1: Overview over the variable parameters investigated in the study. A total of 14 different geometries were investigated.

Experimental

Electrochemical impedance spectroscopy (EIS) has been used to investigate the variables; *defect size*, *l/w ratio* and *coating thickness*. Probes for the experiments were embedded in resin to avoid delamination of a coating or crevice corrosion. They can be seen in Figure 2. Variable coating thicknesses where made by punching a 1cm^2 hole in a 0.5mm thick tape and adding layers to the 1cm^2 circular probe until thicknesses of 1, 3 and 10mm were reached. Prior to the experiment, the probes were polished to a grid 220, obtaining a fresh metal surface.

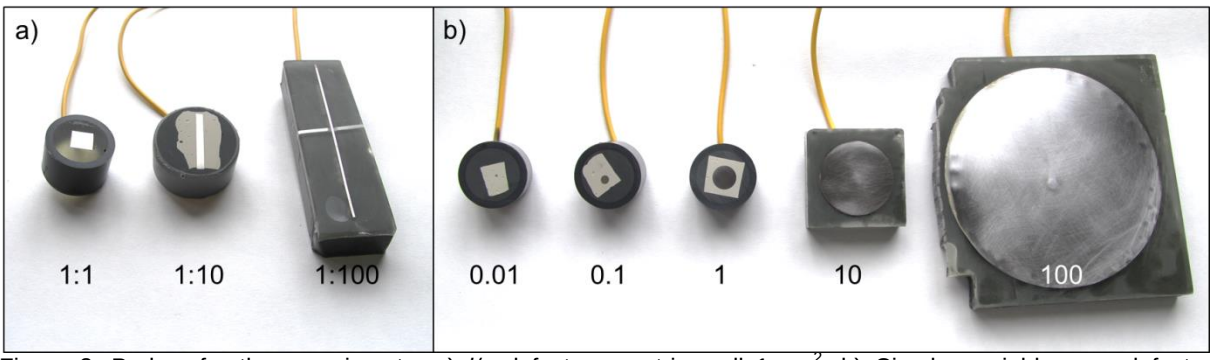

Figure 2: Probes for the experiments. a) *l/w*-defect geometries, all 1 cm^2. b) Circular variable area defects, numbers in cm^2.

A standard three-electrode setup was used, with the coating defect as the working electrode, an inert counter electrode mesh surrounding the working electrode and a standard calomel electrode as the reference electrode connected to the setup via a Luggin capillary placed in front of the working electrode. The working electrode was put in an upright orientation according to Figure 1. For each geometry, 400 mL of non-scaling artificial soil (NAS) solution prepared according to Table 1 was transferred to a beaker and de-aerated by bubbling through with nitrogen gas for >30 min. prior to the experiment. For the 100 cm^2 sample a larger beaker and 1800 mL was needed, and the bubbling time was extended. The beaker was placed in a grounded faraday cage during the experiment to minimize electromagnetic noise from the surroundings. No stirring was applied during the experiment in order to better simulate the stagnant conditions in soil.

Table 1: Non-scaling Artificial Soil (NAS) solution

Species	Concentration
Na_2SO_4	$5.0 \cdot 10^{-3}$ M
$NaHCO_3$	$2.5 \cdot 10^{-3}$ M
NaCl	$10.0 \cdot 10^{-3}$ M

The measurement sequence comprised 20 min. settling time at increasingly more cathodic E_{on} potentials; OCP, -850 mV, -1000 mV, -1250mV and -1550 mV vs. CSE, each followed by an EIS measurement using a 10 mV AC perturbation in the frequency range 160MHz–16mHz with 7 measurements per decade. A Gamry Instruments Reference 600 Potentiostat was used for the measurements and the data were analysed using the Echem Analyst software package from Gamry.
Electrical Resistance (ER) probes from MetriCorr with a $1cm^2$ rectangular coating defect with a *l/w*-ratio of 10 have been used to investigate the influence of defect orientation. Unlike the impedance measurements these investigations were long-term experiments conducted in a soil-box environment; a 50L plastic box filled with 50kg of inert quartz sand and wetted (approx. 30L) with the NAS solution specified in Table 1. The probe layout in the soil box can be seen in Figure 3, at an intermediate state of filling with sand.

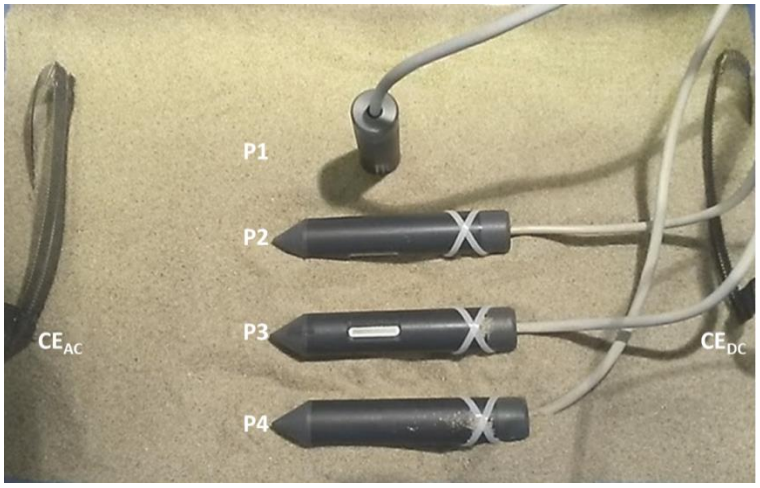

Figure 3: Probe layout in a soil-box for investigating the effect of defect orientation. Probes are marked from 1-4 and AC and DC counter electrodes are also visible on either side.

Two counter electrodes were implemented to separate the experimental DC and AC circuit as described by Goidanich et.al. [5]. During the entire experimental period a U_{ac} = 20V AC perturbation was applied. To ensure enough cathode activity, the E_{on} potential was initiated as low as -1250mV (vs. CSE) and kept there for 4 weeks while corrosion and electrical parameters where monitored with ICL-02i dataloggers from MetriCorr. Subsequently E_{on} was lowered with 100mV with 3 weeks intervals until a potential of -1650mV (vs. CSE) was reached.

EIS Investigations

The electrochemical impedance response from the cell has been fitted to an equivalent circuit as shown in Figure 4, including a solution resistance (or spread resistance), R_s, connected to a parallel coupled charge transfer resistance, R_{ct}, and double layer capacitance represented by a constant phase element, Q. A Warburg

diffusion element is placed in series with R_{ct}, to accommodate a diffusion signal in some of the measurements.

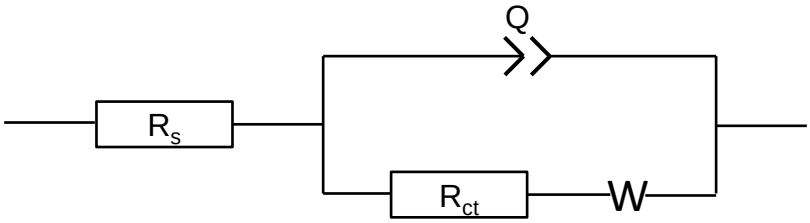

Figure 4: Randles circuit with a Warburg diffusion element.

The impedance response from the elements is given in Table 2, where j is the imaginary unit and ω is the angular frequency. The real frequency is given by $\omega = 2\pi f$.

Table 2: Equivalent circuit elements and their impedance

Equivalent element		Impedance	Parameters
R	Resistor	$Z_R = R$	R
Q	Constant Phase Element	$Z_Q = \frac{1}{Q(j\omega)^n}$	Q, n
W	Warburg Diffusion Element (infinite)	$Z_W = \frac{1}{Y_0\sqrt{j\omega}}$	Y_0

The use of a Q-element allowed for a better fitting, and instead the pseudo-capacitive response C* of the double layer is calculated as (1) for further analysis.

$$C^* = \frac{(R_{ct} \cdot Q)^{\frac{1}{n}}}{R_{ct}} \quad (1)$$

It can be seen that if the value of *n* equals 1, the constant phase element acts as a real capacitor. Furthermore it can be seen that the Warburg element converges to a 'short' for large values of Y_0.
Figure 5 shows how impedance data presented in a) a Nyquist Plot representation and b) a Bode Plot representation.

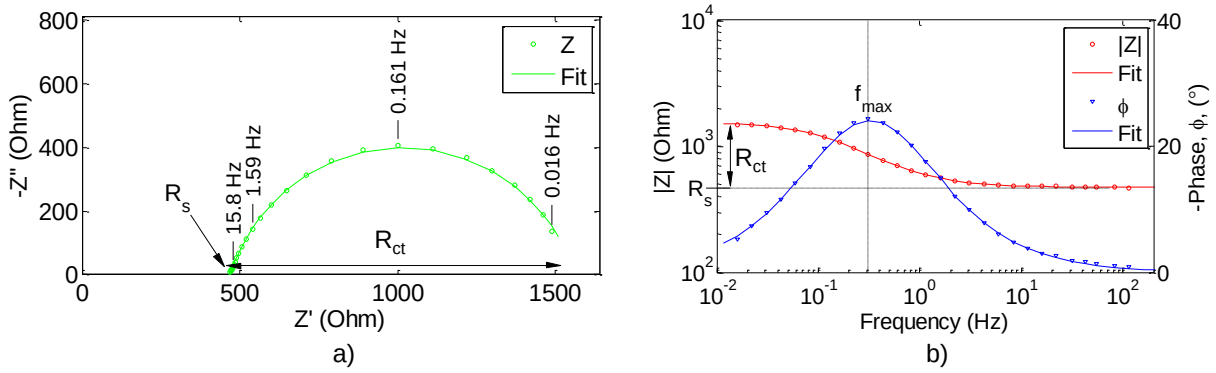

Figure 5: Graphical presentation of impedance data: a) Nyquist plot showing a complex plane representation. b) Bode plot showing the frequency dependent impedance and phase response.

In the Nyquist plot, a Randles circuit without the Warburg element will always produce a semi-circle in the complex plane. The constant phase element will yield a slightly suppressed semi-circle dependent on the value of *n*, and if diffusion is

predominant, the data points will align on a 45° angle line or 'tail' at low frequencies. The Bode plot gives a better understanding of the frequency dependent impedance response. In terms of AC corrosion, it is interesting to observe the response at 50/60Hz.
The fitted values of R_s have been compared to the model reported by Nielsen et.al. [1], which for the present analysis can be simplified to (2) and (3)

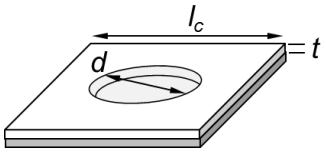

$$R_s = \frac{\rho_{soil}}{2d}\left(1 - \frac{d}{5l_c}\right) + \rho_{pore}\frac{4t}{\pi d^2} \quad (2)$$

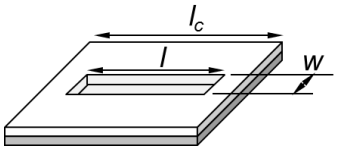

$$R_s = \rho_{soil}\frac{1}{\sqrt{\frac{36}{\pi}(l^2 + w^2)}}\ln\left(\frac{4l}{w} + \frac{4w}{l}\right)\left(1 - \frac{w + l}{10l_c}\right) + \rho_{pore}\frac{t}{lw} \quad (3)$$

Results

Defect orientation

The corrosion rate measured by the ER-technique for coating defects having different orientations is shown in Figure 6. The data markers indicate the direction of the coating defect, i.e. ▌: sideways vertical (P1), ▬: sideways horizontal (P2), ▲: upwards (P3) and ▼: downwards (P4). With increasingly negative polarisation the corrosion rate increases, but the effect is found to be highly dependent on the defect orientation. Lower corrosion rates can be seen for P2 and P4, while P1 and P3 show markedly higher corrosion rates, especially at ≥ -1450 mV. The upright facing defect corrodes at extremely high rates after ≥ -1550 mV (in the order of mm/yr) so the y-axis scale has been adjusted with a factor of 5 past 1000 µm/yr.

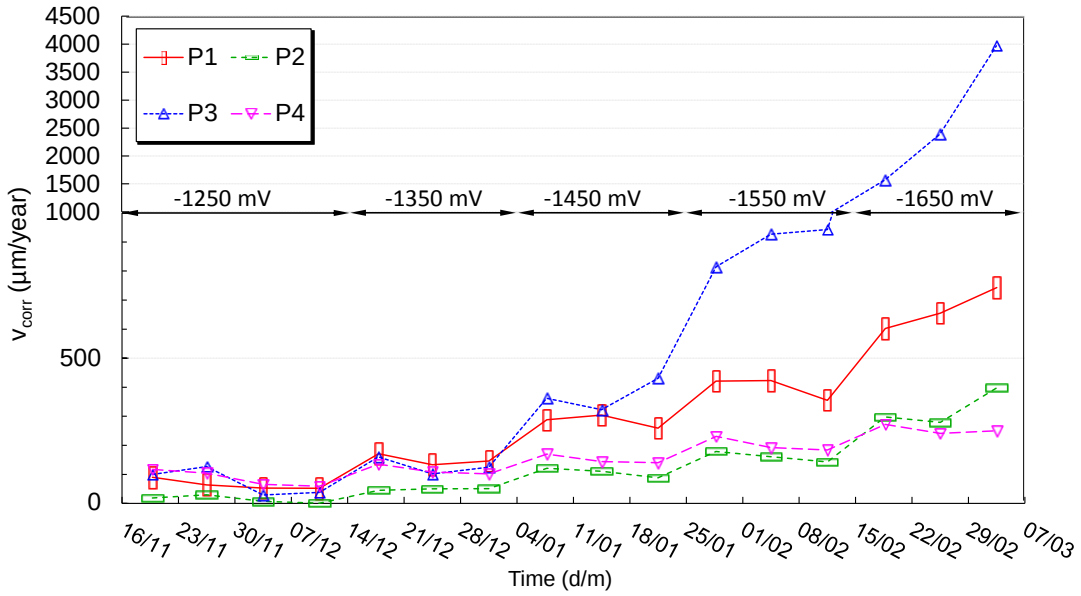

Figure 6: Weekly average corrosion rates for differently oriented probes, indicated by the data marker, as a function of time and E_{on} potential (arrows). Notice the change in scale of the y-axis after 1000 µm/year.

This shows in all clarity that coating defects in the same chemical environment and subject to identical AC and DC voltages responds differently to variations in the CP protection level dependent on their orientation. Figure 7a shows how the spread resistance develops with increasingly negative protection potential for the different defects, Figure 7b illustrates the immediate effect of lowering Rs, i.e. the DC current density increases. The same is true for the AC current density. Figure 7c and d illustrates the correlation between the AC and DC current densities, and the corrosion rate, and as expected the corrosion rate increases with the current densities. Interestingly there appears to be a very simple relation between the DC current density and the corrosion rate, corresponding to a straight line in a double-log plot.

$$v_{corr} = k(-J_{dc})^2 \quad (4)$$

Where *k* is a factor that moves the line up and down in the plot. Here, *k* = 1. This simple relation is likely too simple for universal application, but it outlines very well the 'alkalisation theory' by Nielsen that states that AC corrosion is highly dependent on the cathode reaction (5) and the following alkalisation at the steel surface, which in combination with an AC perturbation causes the steel to fluctuate in and out of the corrosive region in the Pourbaix diagram.

$$2H_2O + 2e^- \rightarrow H_2(g) + 2OH^- \quad (5)$$

To understand why the defect orientation is of importance, reaction (5) is important. Hydrogen gas developing at a surface will always drift upwards, whereas the developed hydroxyl-ions will not. In fact, it is speculated whether increasing concentrations of OH^- will increase the local solution density, causing it to flow downwards.

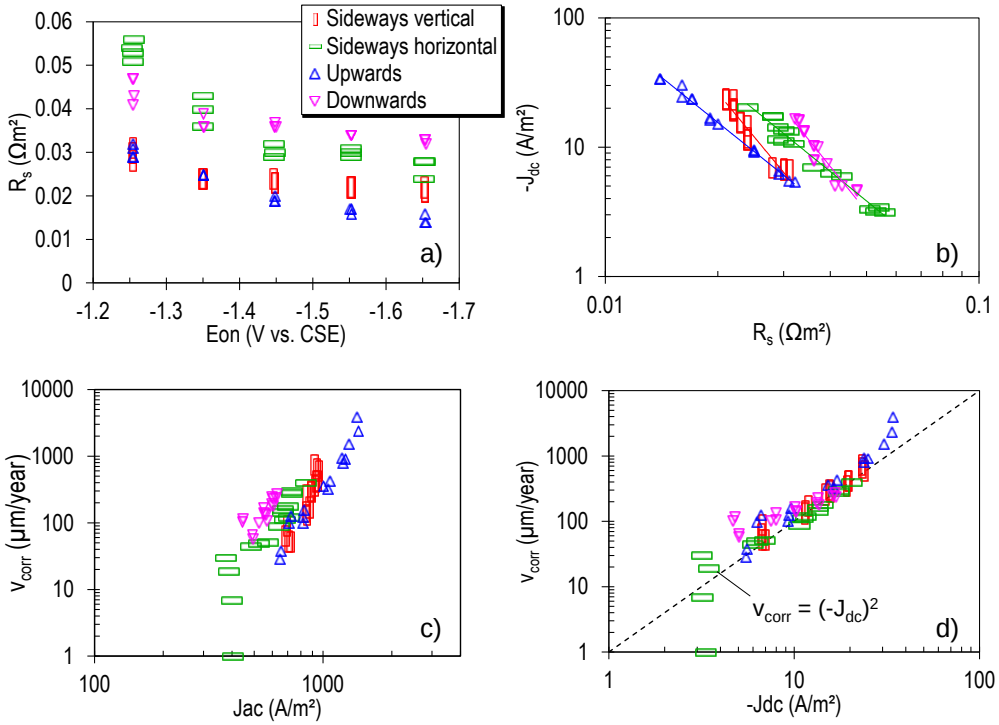

Figure 7: a) The spread resistance drops with the protection potential, but the effect varies with defect orientation. b) The protection current density increases with lower values of Rs. c) the corrosion rate increases with AC current density. d) The corrosion rate falls on an almost straight line in a double-log plot being a function of the DC current density squared.

Assuming that the OH- production at any of the defects is initially the same at a given CP overpotential, there will be a flow away from the downwards oriented defect, whereas the upwards oriented defect will accumulate OH^- and thereby dramatically increase the pH and reduce R_s. With respect to the sideways oriented defects, the concentration of OH- will increase with the flow direction towards the bottom Therefore the vertical defect will experience higher pH and lower R_s locally at the bottom, and AC corrosion rates likewise.

Defect size

Fitting of the large amount of impedance data to the Randles circuit model of the electrode/electrolyte interface in Figure 4, yielded values for R_s, R_{ct}, Q (the constant phase element) and W (the Warburg diffusion element). The latter was included to improve the fitting of the model to the data, but in most cases, no diffusion signal was present and the Y0 value was very high, giving negligible Warburg impedances according to the expression in Table 2. These are not reported in the following.

Figure 8a depicts the found R_s values normalised with respect to the area (multiplied with the area) as a function of the area.

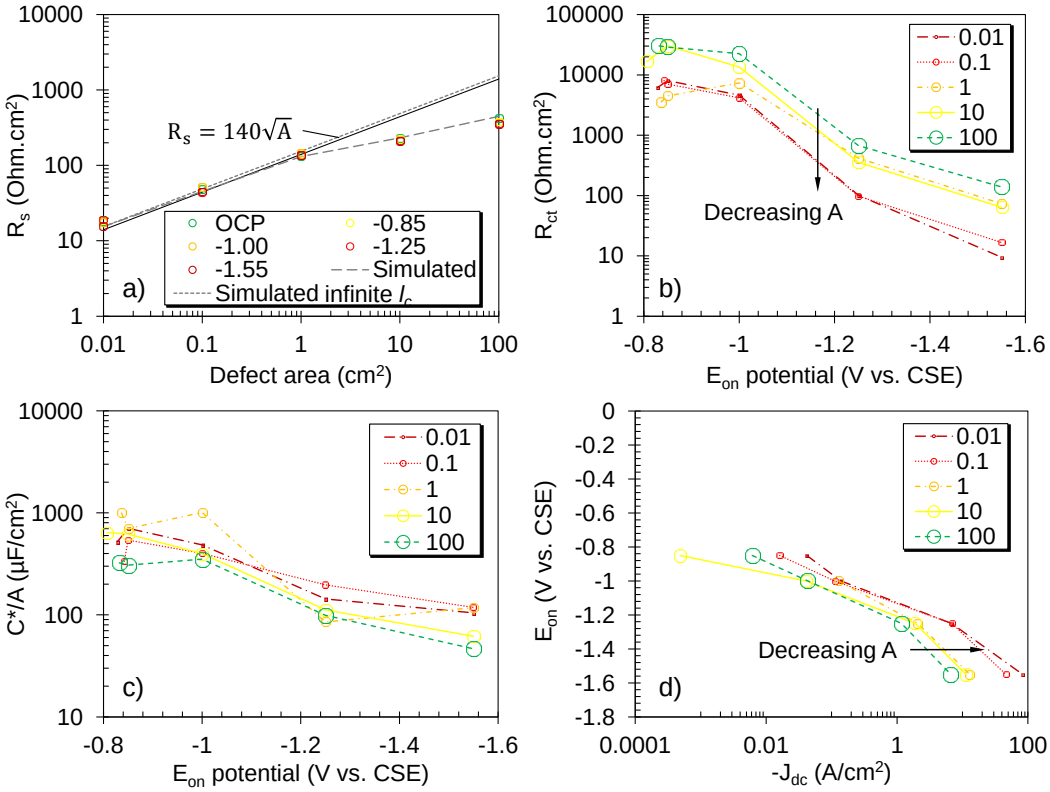

Figure 8: Values from the equivalent circuit modelling for varying defect areas. a) R_s normalised to the area as a function of defect area. b) R_{ct} normalised to the area, as a function of E_{on} potential, comparable to the polarisation behaviour of the electrode. c) Pseudo capacitance, C*, normalised to the area as a function of the E_{on} potential. d) Potentiostatic polarisation curve for the averaged current density measured during the 20 minutes polarisation prior to EIS measurements.

A straight line corresponding to $R_s = 140\sqrt{A}$ is drawn. This correlation was found by Nielsen using EIS in a previous study similar to the present [6], where defect areas from 0.01cm^2 to 4cm^2 were investigated. A dotted line almost on top of it corresponds to the model in (2) having infinite carrier plate size, t = 0 and $\rho_{soil} = 3.5\Omega m$. The stippled line in Figure 8a corresponds to the model in (2), with the actual values for l_c

inserted, and the factor in front of l_c changed from 5 to 1.3, indicating a stronger influence from the carrier plate shielding than the model from [1] predicts. This illustrates that the coupon design is of great importance when simulating coating defects with coupons, and that the 10 and 100cm^2 coupons in this study should have been designed with a bigger l_c to simulate an actual pipeline defect, for which $l_c \cong \infty$. No significant effect of E_{on} on R_s is evident.

Figure 8b shows how the charge transfer resistance decreases with increasingly negative potentials. This is a simple polarisation behaviour since R_s + R_{ct} is effectively the DC resistance at $f = 0$, and the Ohmic relation $U(V) = R(\Omega cm^2) \cdot J(A/cm^2)$ holds. The decrease in R_{ct}, which is the resistance towards charge carrying surface reactions taking place, corresponds to passing the hydrogen overvoltage and initiation of reaction (5). This is also illustrated in Figure 8d, a potentiostatic polarisation curve from the averaged current density, J_{dc}, measured during the 20 minutes polarisation prior to EIS measurements. The current density increases with decreasing A, as also R_{ct} decreases with A. This effect is possibly geometrical due to the surface reactions being dependent on diffusion of reacting species from the surrounding electrolyte. A small (point) defect sees diffusion from a semi-sphere, whereas larger defects see a more flat diffusion profile as illustrated in Figure 9. The volume of electrolyte providing reacting species is thus smaller per active area.

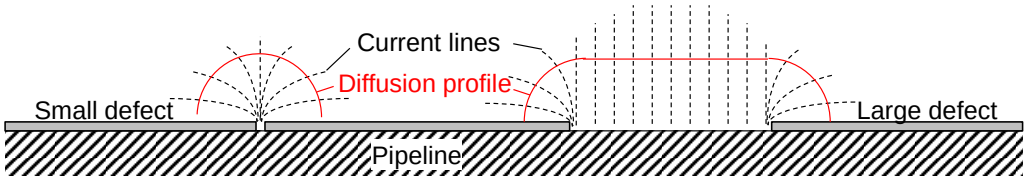

Figure 9: Effect of coating size on the current lines and diffusion profile in the surrounding environment.

Figure 8c shows the pseudo-capacitance normalised with respect to the area as a function of E_{on}. The general equation for a plate capacitor is of the form (6), where *A* and *d* is the area and plate separation respectively and ε is the dielectric constant of the medium in between.

$$\mathrm{C} = \varepsilon \frac{A}{d} \tag{6}$$

Having this in mind, the decreasing area normalised capacitance means that either the dielectric constant of the electrochemical double layer is decreasing, i.e. due to a change in the surface chemistry, or the thickness of the double layer is increasing, e.g. by repulsion of otherwise surface active negative ions such as chlorides from the negatively charged surface, or by generation of H^+-ions and later $H_2(g)$ at the surface which can lift of the surface species. A decreasing capacitance causes an increased impedance of the electrochemical double layer at a given frequency according to (7)

$$\mathrm{Z_C} = \frac{1}{i\omega C} \tag{7}$$

This means that a still larger fraction of the AC current from a given AC perturbation on a coating defect will go through the charge transfer resistance via chemical reactions in the Randles circuit in Figure 4, when the overpotential becomes increasingly negative.

Figure 10 shows the same parameters, but for varying coating thickness. Again a stippled line has been drawn in Figure 10a, corresponding to the model in (2) with $\rho_{soil} = 3.5\Omega\mathrm{m}^2$ and varying coating thickness. The effect of decreasing pore resistivity

is illustrated with an arrow, where the upper line corresponds to $\rho_{soil} = \rho_{pore}$. There is a slight trend that the data points follow this trend with increasingly negative overpotential, but it is not significant. The polarisation behaviour for R_{ct} in Figure 10b, for increasingly negative overpotentials, is again evident, and the decreasing R_{ct} for a thinner coating can be explained by having a larger volume of electrolyte providing reactants for the surface reactions than inside a pore, analogous to the explanation given in Figure 9. The potentiostatic polarisation curves in Figure 10d supports this observation. The decrease in the double layer capacitances in Figure 10c is similar to Figure 8c, and no apparent influence by the coating thickness is evident.

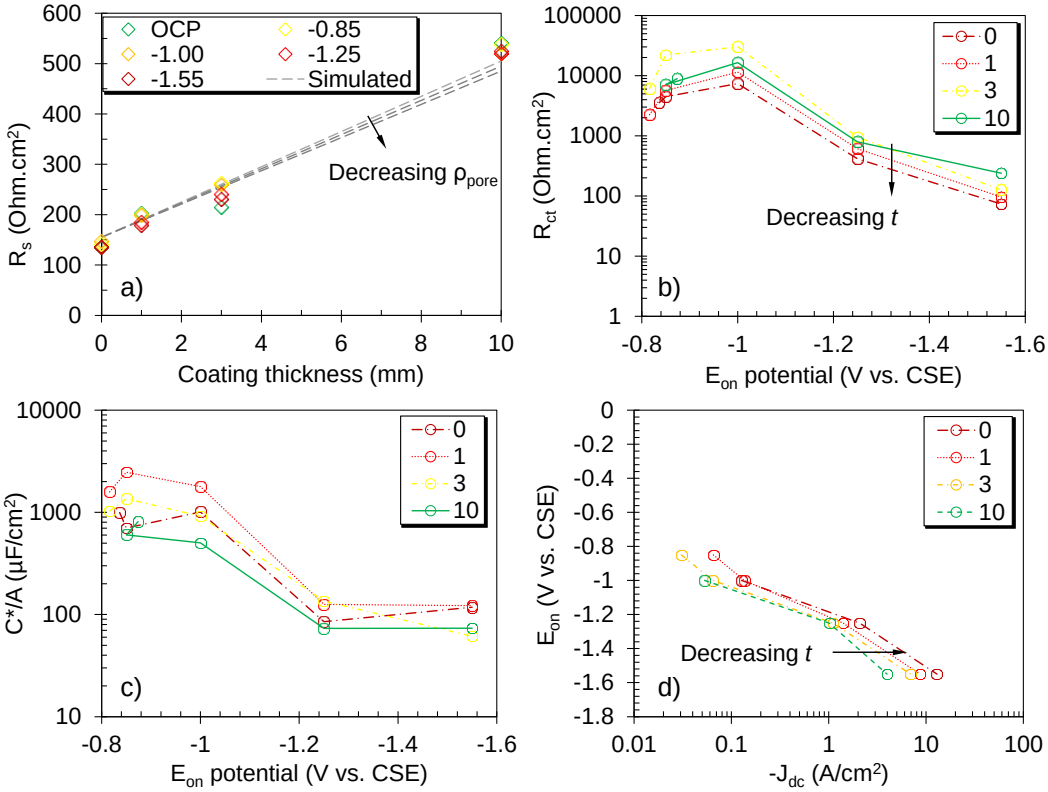

Figure 10: Values from the equivalent circuit modelling for varying coating thicknesses. a) R_s normalised to the area as a function of coating defect. b) R_{ct} normalised to the area, as a function of E_{on} potential, comparable to the polarisation behaviour of the electrode. c) Pseudo capacitance, C*, normalised to the area as a function of the E_{on} potential. d) Potentiostatic polarisation curve for the averaged current density measured during the 20 minutes polarisation prior to EIS measurements.

In Figure 11a the correlation between R_s and the *l*/*w*-ratio can be seen and a simulated curve based on the model in (3) is drawn for t = 0 and $\rho_{soil} = 3.5\Omega\mathrm{m}$ (top curve). The effect of decreasing the soil resistivity is indicated by the arrow. The fit to the model is satisfactory, and shows that even for a fixed coating defect area, the geometry is important in terms of a lower spread resistance for scratch like defects.

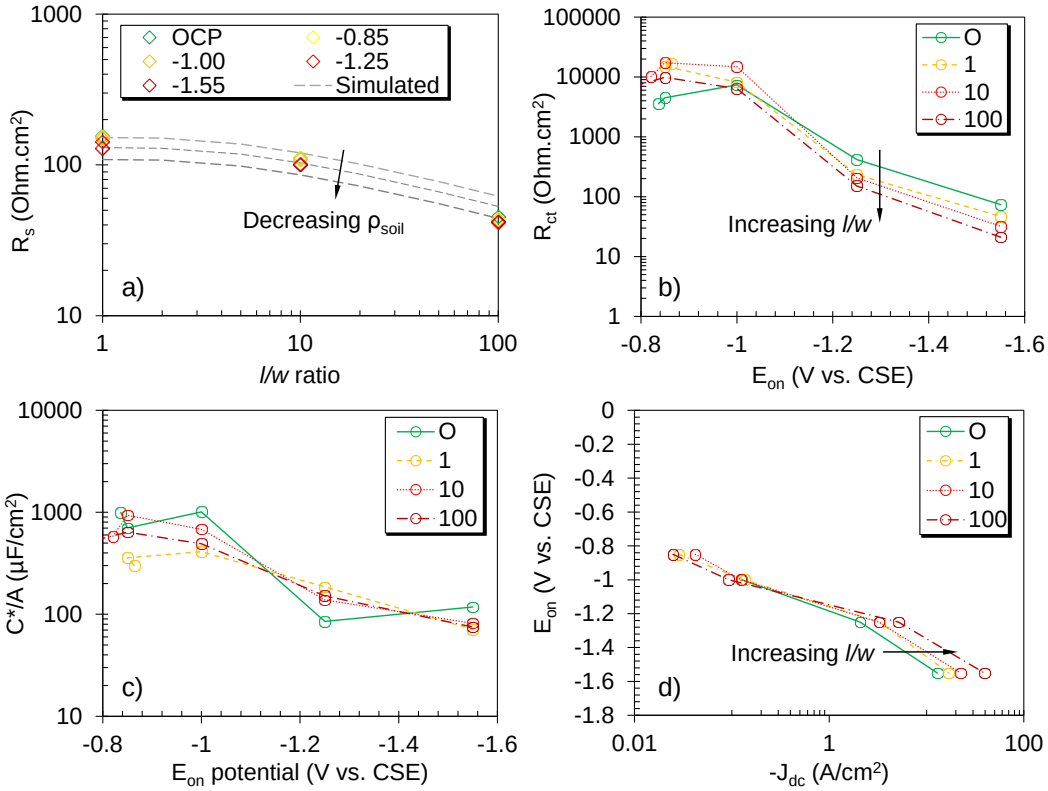

Figure 11: Values from the equivalent circuit modelling for varying *l/w*-ratios. a) R_s normalised to the area as a function of *l/w*-ratio. b) R_{ct} normalised to the area, as a function of E_{on} potential, comparable to the polarisation behaviour of the electrode. c) Pseudo capacitance, C*, normalised to the area as a function of the E_{on} potential. d) Potentiostatic polarisation curve for the averaged current density measured during the 20 minutes polarisation prior to EIS measurements.

R_{ct} decreases with increasing *l/w*-ratio, especially at large overpotentials, as can be seen in Figure 11. Again the explanation is geometrical and analogous to the one given in Figure 9. Diffusion to a long scratch occurs from a larger volume of the electrolyte, than for a point defect having the same active area. The polarisation behaviour in Figure 11d shows an increased J_{dc} with higher *l/w*-ratios accordingly. The trend for the area normalised capacitance is similar to the defect size and coating thickness, i.e. a decreasing C* with negative overpotential, seemingly unaffected by the *l/w*-ratio.

Discussion and Conclusion

The investigations carried out in this study comprises two parallel investigations:

- Long-term measurements of the corrosion rate for coupons having different orientations in a soil-box setup under AC and DC voltage control, measured by the ER-technique.
- Short-term investigations of the electrochemical equivalent circuit describing the electrode/electrolyte interface of different defect geometries in a stagnant aqueous solution under DC control, using the EIS-technique.

One might argue that the latter does not provide information about AC corrosion properties, since no AC perturbation was applied, apart from a small measurement signal. However, while no direct information about AC corrosion rates are obtained, an equivalent circuit for the electrochemical double layer has been determined, and a better understanding of the response of various geometries to AC and DC perturbation is achieved. ER measurements have confirmed well known correlations

between key parameters such as the spread resistance, R_s, the AC and DC current densities, J_{AC} and J_{DC}, and knowing the electrochemical equivalent circuit for an interface allows for a qualified estimation of the AC corrosion performance of this interface.

It has been established that R_s is decreasing for higher levels of cathodic protection in long-term experiments (Figure 7a), and that this is highly influenced by the defect orientation. This suggests that cathode reactions can locally change the solution resistivity, and that the formed species are influenced by orientation, i.e. gravity or a directionally dependent diffusion. Upwards facing defects develops the lowest resistivity suggesting a developed species heavier than water. It is speculated whether OH^- -ions are the main contributor, but further experiments are needed to confirm that OH^- does in fact drift downwards, and that no other species are more influential.

With decreasing Rs, AC and DC current densities increases, and ER measurements show increasing corrosion rates correspondingly. In fact the DC current density appears to be the most influential, showing a very strong correlation to the corrosion rate given in (4).

Investigations of the coating defect geometries have revealed that both the spread and the charge transfer resistance, R_s and R_{ct}, are dependent on defect size, coating thickness and *l/w*-ratio. Knowing that these factors have a great influence on the AC corrosion properties, it is important to be aware of this when using coupons for AC corrosion assessments. Also the coupon design, i.e. carrier plate dimensions, have been found to have an influence, and a revision of known models [1] has been made, based on experimental data.

The findings suggests that smaller, scratch-like defects with a very thin adjacent coating yields the smallest R_s and R_{ct} values, and would therefore be more vulnerable to AC corrosion.

The pseudo-capacitance of the electrochemical double layer has not been found to be markedly influenced by coating defect geometry, but to a larger degree by the cathodic protection overpotential. This yields a higher impedance of the electrochemical double layer at any given frequency with increasingly negative overpotentials, and thus a larger part of the AC current density from an AC perturbation will go through charge carrying reactions. This could be iron dissolution during the anodic half-cycle of the AC perturbation, and the change in AC corrosion rate found using the ER-technique with increasing CP overpotentials could perhaps be attributed to this effect.

Bibliography

[1] L. V. Nielsen, M. Berggreen, L. Bortels and J. Parlongue, “Effect of Coating Defect Size , Coating Defect Geometry , and Cathodic Polarization on Spread Resistance : - Consequences in relation to AC Corrosion Monitoring,” in *CeoCor*, Bruges, 2010.

[2] M. Büchler, C. Voûte and H. Schöneich, “EFFECT OF CATHODIC PROTECTION LEVELS AND DEFECT GEOMETRY ON THE A . C . CORROSION ON PIPELINES,” 2007.

[3] M. Büchler, “Discussion of the mechanism of a.c.-corrosion of cathodically protected pipelines: The effect of the cathodic protection level,” in *CeoCor*, Slovakia, 2008.

[4] M. Büchler, C. Voûte and H. Schöneich, “The Effect of Variation of AC-Interference over time on the Corrosion of Cathodically Protected Pipelines,” in *CeoCor Sector A*, Vienna, 2009.

[5] S. Giodanich, L. Lazzari and M. Ormellese, “AC Interference Effects on Polarized Steel,” p. 12, 2003.

[6] L. V. Nielsen, “EIS Investigation of the Randles Circuit Elements for Carbon Steel Exposed in Artificial Soil Solution,” Technical University of Denmark & DONG Natural Gas A/S, Lyngby, 2000.